Discovery and characterization of H_v1-type proton channels in reef-building corals.

Gisela E. Rangel-Yescas[1], Cecilia Cervantes[1], Miguel A. Cervantes-Rocha[1], Esteban Suarez-Delgado[1], Anastazia T. Banaszak[2], Ernesto Maldonado[2], Ian. S. Ramsey[3], Tamara Rosenbaum[4] and León D. Islas[1*]

From:

[1]Departmento de Fisiología, Facultad of Medicina, Universidad Nacional Autónoma de México, Mexico City, Mexico

[2]Unidad Académica de Sistemas Arrecifales, Instituto de Ciencias del Mar y Limnología, Universidad Nacional Autónoma de México, Puerto Morelos, Quintana Roo, Mexico

[3]Department of Physiology and Biophysics, School of Medicine, Virginia Commonwealth University, Richmond, VA, USA

[4]Departmento of Neurociencia Cognitiva, Instituto de Fisiología Celular, Universidad Nacional Autónoma de México, Mexico City, Mexico

*Correspondence to:

León D. Islas, PhD

Departmento de Fisiología

Facultad de Medicina, UNAM,

Ciudad Universitaria, Circuito Escolar S/N

Ciudad de México, 04510, México

leon.islas@gmail.com

Abstract

Voltage-dependent proton-permeable channels are membrane proteins mediating a number of important physiological functions. Here we report the presence of a gene encoding for H_v1 voltage-dependent, proton-permeable channels in two species of reef-building corals. We performed a characterization of their biophysical properties and found that these channels are fast-activating and modulated by the pH gradient in a manner that makes them interesting models for studying these processes more easily. We have also developed an allosteric gating model that provides mechanistic insight into the modulation of voltage-dependence by protons. This work also represents the first functional characterization of any ion channel in scleractinian corals. We discuss the implications of the presence of these channels in the membranes of coral cells in the calcification and pH regulation processes and possible consequences of ocean acidification related to the function of these channels.

Introduction

Voltage-gated, proton-permeable channels are formed by a voltage-sensing domain encoded by the H_v1 protein (Sasaki et al., 2006; Ramsey et al., 2006). These channels are different from canonical voltage-gated channels in that both voltage-sensing and permeation are mediated through a single protein domain. Several functional properties of these channels are also distinct. Most proton permeable channels seem to have evolved to extrude protons from the cell, and towards this end, their voltage dependence is tightly modulated by the proton gradient between extracellular and intracellular solutions (Cherny et al., 1995). These channels seem fundamental in handling fluctuations in intracellular pH and take part in several well-characterized physiological processes that depend on proton concentration changes, such as intracellular pH regulation, sperm flagellum beating, ROS production and bacterial killing in immune cells, initiation of bioluminescence in single-celled algae, etc (Castillo et al., 2015).

H_v1 channels are formed by a protein fold that is structurally equivalent to the voltage-sensing domains (VSDs) of canonical voltage-gated channels. The VSD is formed by a bundle of four antiparallel alpha helices (Takeshita et al., 2014b). The proton conductance of the single H_v1 channels is very small (Cherny et al., 2003), so much so that single-channel recordings are not possible. This has contributed to the proton permeation mechanism being

the least understood property of these channels. However, voltage-sensing is thought to occur through the interaction of charged amino acid side chains with the electric field, leading to outward movement of the fourth domain or S4, in a similar fashion to other voltage-sensing domains (Carmona et al., 2018; De La Rosa and Ramsey, 2018). This outward movement of the S4 is coupled to protons moving through the VSD in a manner that is not completely understood (Randolph et al., 2016).

The range of voltages over which channel activation occurs is strongly modulated by the transmembrane proton gradient, characterized by: $\Delta pH = pH_o - pH_i$ i.e., the difference between external and internal pH. In the majority of known H_v1 channels, the voltage at which half the channels are activated, the $V_{0.5}$ or the apparent threshold for channel opening (V_{Thr}), shifts by roughly 40 mV per unit of ΔpH. Thus, the pH gradient strongly biases the voltage-independent free energy of channel activation (Cherny et al., 1995). With few exceptions, channel activation occurs at voltages that are more positive than the reversal potential for protons, implying that protons are always flowing outward under steady-state conditions. The fact that most H_v1s mediate outward currents is the reason these channels are mostly involved in reversing intracellular acidification or producing voltage-dependent cytoplasmic alkalization (Lishko and Kirichok, 2010; DeCoursey, 2013).

Although a number of studies have delineated the physiological roles of H_v1 voltage-gated proton channels in vertebrate cells (DeCoursey, 2013), less is known about their role in invertebrates. They are potential mediators in processes that are critically dependent on proton homeostasis. As an example, they have been shown to be involved in regulating the synthesis of the calcium carbonate skeleton in coccolithophores, calcifying unicellular phytoplankton (Taylor et al., 2011).

A critical geochemical process facilitated by biology is calcification in corals. Scleractinian or stony corals are organisms in the phylum Cnidaria that deposit calcium carbonate in the form of aragonite to build an exoskeleton. This process has been shown to be modulated by the pH of the solution in which calcium carbonate is precipitated, the so called calicoblastic liquor of fluid (Allemand et al., 2011). The molecular details of pH regulation in corals and its implications for coral calcification are not understood. Although involvement of proton-pumps has been postulated and is likely to be part of proton transport in corals (Tresguerres

et al., 2017), we hypothesized that proton channels might be fundamental to this physiological process and also required for calcification in hard corals. Here we report the presence of genes encoding for H_v1 channels in two species of reef-building corals and we clone and characterize the biophysical properties of these channels in an expression system using patch-clamp electrophysiology. The demonstration of the presence of voltage-gated proton channels in corals is an initial step to a deeper understanding of coral calcification and its dysregulation under ocean acidification conditions. We show that some of the coral H_v1's biophysical properties are different from other known proton channels and this behavior make them interesting models to try to understand some basic biophysical mechanisms in these channels. To explain this behavior, we develop a novel activation model to describe voltage- and pH-dependent gating that has general applicability to H_v1 channels.

Materials and methods

Identification of H_v1 sequences and cloning. The transcriptome of the Indo-Pacific coral *Acropora millepora* (Moya et al., 2012) was searched for sequences coding for putative voltage-sensing residues present in canonical H_v1 channels with the form: RxxRxxRIL, which corresponds to the S4 segment, an essential part of H_v1 channels and other voltage-sensitive membrane proteins. Blast searches detected four sequences that we identified as belonging to a putative proton-permeable channel. The GenBank accession numbers for these are: XM_015907823.1, XM_015907824.1, XM_029346499.1 y XM_029346498.1. We designed two pairs of oligonucleotides to amplify two of these sequences (Table 1). Total RNA was extracted from tissue from fragment of *Acropora millepora* obtained from a local salt-water aquarium provider. RNA was extracted by dipping the whole fragment for 2 min in 5 ml of solution D (4 M guanidinium thiocyanate, 25 mM sodium citrate, 5 % sarkosyl and 0.1 M 2-mercaptoethanol). After incubation, tissue was removed by gently pipetting the solution for 2 min. At this point, the calcareous skeleton was removed and RNA extraction continued according to (Chomczynski and Sacchi, 1987). Total RNA (1 µg) from *A. millepora* was used for RT-PCR, employing oligo dT and SuperScripII reverse transcriptase (Invitrogen). Complementary DNA obtained from RT-PCR was used in three PCR reactions using oligos: 1) AcHv1Nter5´ and 3´; 2) AcHv1Cter5´ and 3´ and, 3) AcHv1Nter5´ and AcHv1Cter3´ (Table

1). The Platinium Pfx DNA polymerase (Invitrogen) was used for amplification according to the manufacturer's instructions. 1 µl of Taq DNA polymerase (Invitrogen) was used for 10 min at 72 ºC to add a poly A tail at 5' and 3' ends and facilitate cloning into the pGEM-T vector. The PCR reaction 3 gave rise to a full open reading frame (ORF) containing AmH_v1. New oligos AcHv1Nter5´ and AcHv1Cter3´ containing restriction sites Kpn1 and Not1 respectively were used to re-amplify the ORF in pGEM-T and subclone it into pcDNA3.1 for heterologous expression.

The H_v1 channel from *A. palmata* was cloned from a fragment of an adult specimen collected in the Limones Reef off of Puerto Morelos, Mexico. RNA extraction from small coral pieces was carried out by flash freezing in liquid nitrogen and grinding the frozen tissue. All other cloning procedures were as for *A. millepora.* All clones were confirmed by automatic sequencing at the Molecular Biology Facility of the Instituto de Fisiología Celular at UNAM.

Heterologous expression of AmH_v1. The cloned AmH_v1 was expressed in HEK293 cells. HEK293 cells were grown on 100 mm culture dishes with 10 ml of Dulbecco´s Modified Eagle Medium (DMEM, Invitrogen) containing 10 % fetal bovine serum (Invitrogen) and 100 units/ml-100 µg/ml of penicillin-streptomycin (Invitrogen), incubated at 37°C in an incubator with 5.2 % CO_2 atmosphere. When cells reached 90 % confluence, the medium was removed, and the cells were treated with 1 ml of 0.05 % Trypsin-EDTA (Invitrogen) for 5 min. Subsequently, 1 ml of DMEM with 10 % FBS was added. The cells were mechanically dislodged and reseeded in 35 mm culture dishes over 5x5 mm coverslips for electrophysiology or in 35 mm glass bottom dishes. In both cases, 2 ml of complete medium were used. Cells at 70 % confluence were transfected with pcDNA3.1-AmH_v1 prepared from a plasmid midiprep, using jetPEI transfection reagent (Polyplus Transfection). For patch-clamp experiments, pEGFP-N1 (BD Biosciences Clontech) was cotransfected with the channel DNA to visualize successfully transfected cells via their green fluorescence. Electrophysiological recordings were done one or two days after transfection.

*Electrophysiology***.** Proton current recordings were made from HEK293 cells expressing pCDNA3.1-AmH_v1 in the inside-out, whole-cell and outside-out configurations of the patch-clamp recording technique. For whole-cell and inside-out recordings, the extracellular

solution (bath and pipette, respectively) was (in mM): 80 TMA-$HMESO_3$, 100 buffer (MES: pH 5.5, 6.0 and 6.5; HEPPES: pH 7.0, 7.5), 2 $CaCl_2$, 2 $MgCl_2$ and pH adjusted NMDG/TMAOH and HCl. The intracellular solution (pipette and bath respectively) was (in mM): 80 TMA-$HMESO_3$, 100 buffer (MES: pH 5.5, 6.0 and 6.5; HEPES: pH 7.0, 7.5), 1 EGTA and pH adjusted NMDG/TMAOH and HCl.

Conditions for recording zinc effects. The effect of zinc was evaluated in outside-out patches at a ΔpH of 1. The bath solution composition was (in mM): 100 TMA-$HMESO_3$, 100 HEPES, 8 HCl, 2 $CaCl_2$, 2 $MgCl_2$, and the indicated concentration of $ZnCl_2$. The pipette solution was (in mM): 100 TMA-$MESO_3$, 100 MES, 8 HCl, 10 EGTA and 2 $MgCl_2$. Both solutions were adjusted to pH 7 and pH 6 respectively with TMA-OH/HCl. Patches were placed in front of a perfusion tube that was gravity-fed with the appropriate solution. Tubes were changed with a home-built rapid perfusion system.

Macroscopic currents were low-pass filtered at 2.5 kHz, sampled at 20 kHz with an Axopatch 200B amplifier (Axon Instruments, USA) using an Instrutech 1800 AD/DA board (HEKA Elektronik, Germany) or an EPC-10 amplifier (HEKA Elektronik, Germany). Acquisition control and initial analysis was done with PatchMaster software. Pipettes for recording were pulled from borosilicate glass capillaries (Sutter Instrument, USA) and fire-polished to a resistance of 4-7 MΩ when filled with recording solution for inside- and outside-out recordings and 1-3 MΩ for whole-cell. The bath (intracellular) solutions in inside-out patches were changed using a custom-built rapid solution changer. For whole-cell recordings all the bath solution was exchanged to manipulate pH. In some recordings, linear current components were subtracted using a p/4 subtraction protocol.

Data analysis. Conductance, G, was calculated from I-V relations assuming ohmic instantaneous currents, according to:

$$I(V) = G \cdot (V - V_{rev})$$

The normalized conductance-voltage (G-V) relations were fit to a Boltzmann function according to equation 1:

$$\frac{G}{G_{max}} = \frac{1}{1+\exp\left(\frac{q(V-V_{0.5})}{K_B T}\right)} \qquad \text{Equation 1.}$$

Here, $V_{0.5}$ is the voltage at which G/G_{max} = 0.5, q is the apparent gating charge (in elementary charges, e_o) and K_B is the Boltzmann constant and T temperature in Kelvin (22°C).

The time constant of activation was estimated via a fit of the second half of currents to the equation:

$$I(t) = I_{ss} \cdot \left(1 - \mathrm{e}^{\left(\frac{-(t-\delta)}{\tau}\right)}\right) \qquad \text{Equation 2.}$$

Where I_{ss} is the amplitude of the current at steady-state, δ is the delay of the exponential with respect to the start of the voltage pulse and τ is the time constant, both with units of ms. The voltage-dependence of δ and τ were estimated from a fit to equation:

$$k(V) = k(0)e^{(-Vq_k/K_B T)} \qquad \text{Equation 3.}$$

Where k stands for δ or τ and $k(0)$ is the value of either parameter at 0 mV.

Currents in the presence of zinc were normalized to the current before application of the ion to obtain a normalized fraction of current blocked as: F_B= 1-I/I_{max}. The zinc dose response curve was fitted to Hill's equation in the form:

$$F_B = \frac{1}{1+\left(\frac{K_D}{[Zn]_o}\right)^{n_H}} \qquad \text{Equation 4.}$$

K_D is the apparent dissociation constant, $[Zn^{2+}]_o$ is the extracellular zinc concentration and n_H is the Hill coefficient.

Results

We have identified the presence of short DNA sequences in the genome of the Indo-Pacific reef-building coral *Acropora millepora,* that correspond to a gene encoding the H_v1 voltage-activated proton-selective ion channel (Ramsey et al., 2006; Sasaki et al., 2006). We proceeded to clone this gene from mRNA obtained from tissue of a small specimen of *A. millepora* and refer to this sequence as AmH_v1 or H_v1-type proton channel of *Acropora millepora*. As expected, the protein sequence has similarity to several other H_v1 genes from varied organisms. The least degree of conservation appears when comparing this sequence to the dinoflagellate *Karlodinium veneficum* H_v1 channel (Figure 1A). Secondary structure prediction suggests that AmH_v1 is a canonical H_v1 channel formed by a voltage-sensing

domain with four transmembrane segments. The protein sequence was used for 3D modeling using the SWISS MODEL server (Waterhouse et al., 2018), which produced models based on the H_v1 chimera structure (Takeshita et al., 2014a) and the Kv1.2 potassium channel voltage-sensing domain (Long et al., 2005). This structural model is shown in Figure 1B. The predicted model indicates a shortened N-terminal region, four transmembrane domains and a long C-terminal helix. This helix is predicted to engage in a coiled-coil (Paircoil2 (McDonnell et al., 2006) as has been shown in human (hH_v1) and in the sea squirt *Ciona* VSOP/H_v1 (Sasaki et al., 2006).

A search of available transcriptomes from several coral species allowed us to detect the presence of sequences that seem to correspond to H_v1 channels. This suggests that H_v1 proton channels might be found in many families of scleractinian corals (Supplementary Figure 1).

We were interested in knowing if the same gene is present in a closely related species from the Caribbean Sea. Thus, we used the same primers to clone the H_v1 channel from *Acropora palmata*, a widespread coral in the same family and which we call ApH_v1. The amino acid sequence is almost identical to AmH_v1 (Supplementary Figure 2), the greatest divergence is found between a few amino acid residues in the C-terminal region. This result suggests that despite the large biogeographic difference, these two genes have not diverged significantly. The ApH_v1 sequence also gives rise to fast-activating voltage-gated proton currents (Supplementary Figure 2).

A

```
AcHv1            --------------------MIDARTRRSSMDDQLPADELKEMGQPGTTAAVM-------
N.vectensis      -------------------MESDNQQLVGQLVFDTQSLGERAMDKEIEVEVGD-------
C.sculpturatus   -----------------------------MKMDSGQEKNNISVKKVENAKEDC-------
Human            MATWDEKAVTRRAKVAPAERMSKFLRHFTVVGDDYHAWNINYKKWENEEEEEEEEQPPPT
M.musculus       MTSHDPKAVTRRTKVAPTKRMSRFLKHFTVVGDDYHTWNVNYKKWENEEEEEE----PAP
K.veneficum      -----------------MDRILHHAVHTVHTSKSARDAEGHGTWQSKLNEALN-------
                                                  .

                                                                   S1
AcHv1            ---------ASTVCLTEDDTECPANKNHREKLNELLHGDKIQYAIVVLVIIDIIIVIAEL
N.vectensis      ---------GGGDAQVVSSTPCWHILKDRPRLCEIIHGQKAQYTIIALVIIDCIIVIAEL
C.sculpturatus   ---------ISASTDFEVDVDLRPYITFQERLCKILHSHKFQVIIISLVIFDCLLVISEL
Human            PVSGEEGRAAAPDVAPAPGPAPRAPLDFRGMLRKLFSSHRFQVIIICLVVLDALLVLAEL
M.musculus       TSAEGEGNAEGPDAEAGSASTPRQSLDFRSRLRKLFSSHRFQVIIICLVVLDALLVLAEL
K.veneficum      ---------SSKVHTILNVLLICDLMTVIIGMLLEQYYSDSQVQGLTEAFKDCLEKRTFC
                           .                    :         *   :  .. * :   :

                                       S2                                S3
AcHv1            VLDLRAGSEH-HDN-SASHVLHYISIAILSVFMIELLLKIYAMGFTFFKHKMEVFDGFVI
N.vectensis      LVDLEILKVH-HDN-PAPHILHDVSIAILSLFIIELIVKIYAMGMEFFHHKLEVFDGIVV
C.sculpturatus   MIDLEIVPLG-DEHHIAPHVLHYMSIFILSLFIIEISAKIYAFRKEFFLHKLEVFDAIVV
Human            ILDLKIIQPD-KNN-YAAMVFHYMSITILVFFMMEIIFKLFVFRLEFFHHKFEILDAVVV
M.musculus       LLDLKIIEPD-EQD-YAVTAFHYMSFAILVFFMLEIFFKIFVFRLEFFHHKFEILDAFVV
K.veneficum      PDPSHLAHYGNHDLHEWAERMEYASLAILLIFLLENMLLVLANGCRFFANPFHILDIVVV
                       .      .:      :.  *: ** .*::*   : .     ** : :.::* .*:

                                         S4
AcHv1            IVSFALDIAFSNEQGGVDGVSLIVLLRLWRVTRIVNGIILSVQMRAEKKVQAVMKENAEL
N.vectensis      IVSFALDIAFSGGN-AAEGASLLIIILRLWRVTRIVNGIILSVKMQDEKKIHHLHKVIEEL
C.sculpturatus   VLSFSLDIAFRNSSGAINGSGLIIIILRLWRVARILNGIVLSVKTQAEHKLSKEIQLREAV
Human            VVSFILDIVLLFQEHQFEALGLLILLRLWRVARIINGIIISVKTRSERQLLRLKQMNVQL
M.musculus       VVSFVLDLVLLFKSHHFEALGLLILLRLWRVARIINGIIISVKTRSERQILRLKQINIQL
K.veneficum      VVSVGFELQGILGEGHDAGIGLVVFARTWRFIRLGHGIHEMHEEHEAEDHGEHRVSDAAG
                 ::*. :::     .    . .*::: * **. *: :**     : :   ..

AcHv1            KTELEQLKSKCAQLESELTTLKQS------------------------------------
N.vectensis      QEELDRLKTRNAELENELKTLKGTKEEPVAEEATT-------------------------
C.sculpturatus   EQELAKCRNYCAALEQEVESLRSVLKMNNIKELPPTVINKPVLQHNTVNVVAEVNNATVH
Human            AAKIQHLEFSCSEKEQEIERLNKLLRQHGLLGEVN-------------------------
M.musculus       ATKIQHLEFSCSEKEQEIERLNKLLKQNGLLGDVN-------------------------
K.veneficum      SLEAPLQKGSFEQHAKGTSGVHHARSQASSNREGREGCCVQ-------------------
                   :    .      .    :.

AcHv1            -----
N.vectensis      -----
C.sculpturatus   YSNIM
Humano           -----
M.musculus       -----
K.veneficum      -----
```

B

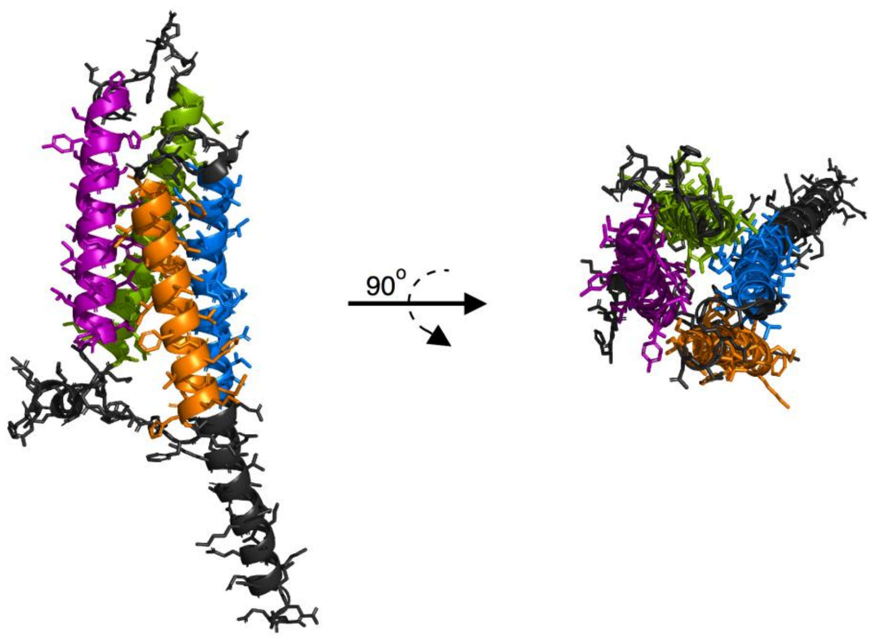

Figure 1

Figure 1. Protein sequence alignment of the *Acropora millepora* H_v1 (AmH_v1) channel with selected H_v1s from other organisms. A) Amino acid sequence alignment of AmH_v1 with other known Hv1 orthologues. The predicted transmembrane domains are shown in colored letters. Stars under the sequence indicate identical amino acids. Double dots indicate conserved amino acids. Single dots indicate charge reversals or amino acids with divergent polarity. B) Predicted structural topology of AmH_v1. Transmembrane domains are colored to correspond with the sequences in A. The left panel is the view parallel to the membrane while the right panel is the view from the top (extracellular) side.

Functional expression of AmH_v1. Voltage-dependence and kinetics.

The cDNA of AmH_v1 was cloned in the pcDNA3 expression vector and transfected into HEK293 cells. Under whole-cell conditions we recorded large voltage-dependent outward currents. Figure 2A shows a family of such currents. The data suggest that these currents were carried mostly by protons, since the reversal potential, measured from a tail current protocol, closely followed the equilibrium potential for protons, as given by the Nernst equation (Figure 2B).

The voltage-dependence of channel gating was estimated from a fit of the normalized conductance vs. voltage to equation 1. The steepness of the curve corresponds to an apparent charge of ~2 e_o, comparable to other H_v1's under similar recording conditions (Figure 2C).

Interestingly, these channels seem to activate rapidly. This is apparent from the current traces, which reach a steady-state within a few hundred ms (Figure 2A), as quantified in Figure 2D. Equation 3 estimates two parameters, an activation time constant (τ) and a delay (δ). Both the time constant and the delay are similarly voltage-dependent at positive potentials. The existence of a delay in the time course implies that activation is a multiple state process. The delay magnitude is smaller than the time constant at all voltages, which can be interpreted to mean that the rate limiting step for opening comes late in the activation pathway (Schoppa and Sigworth, 1998).

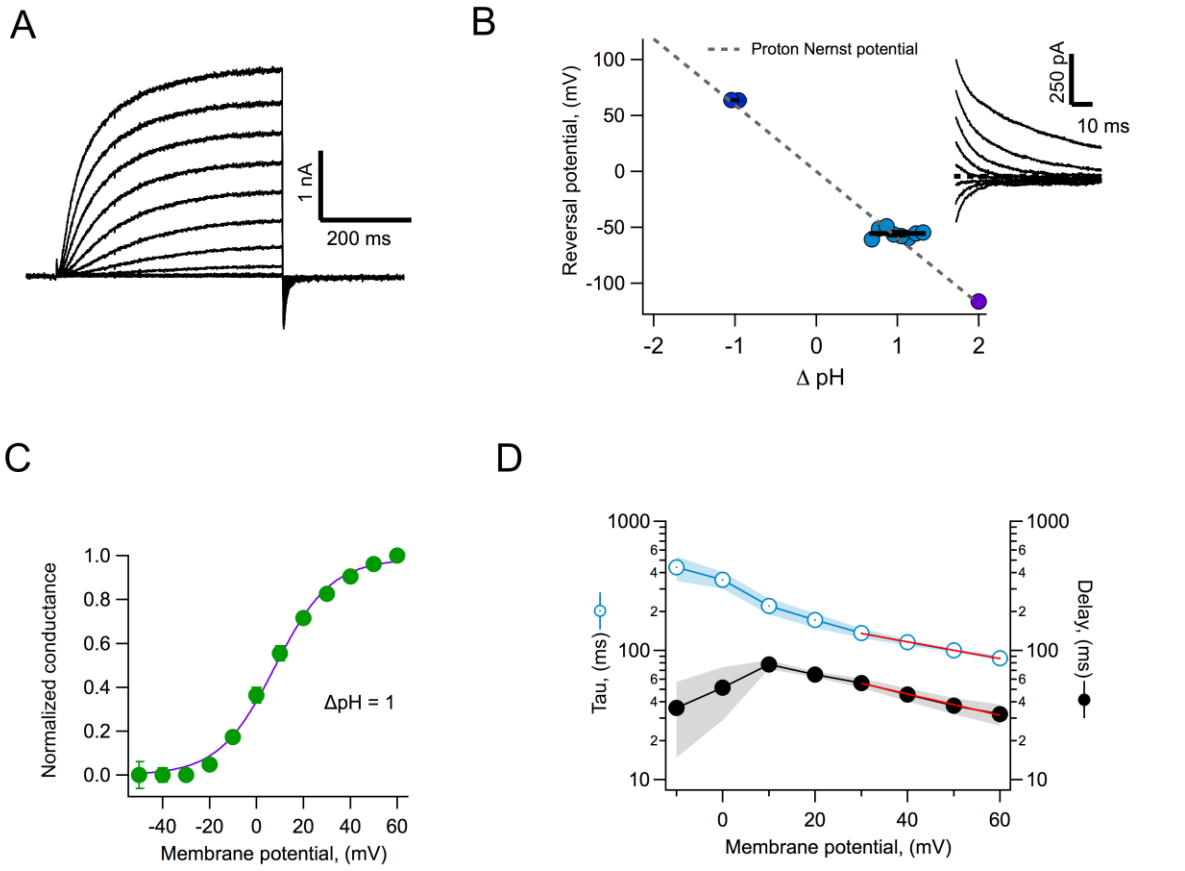

Figure 2

Figure 2. Proton currents mediated by AmH$_v$1 expressed in HEK 293 cells. A) Typical proton current family elicited by depolarizing pulses from -50 to 60 mV in 10 mV intervals. The duration of the pulses is 500 ms. Linear current components have been subtracted. B) Reversal potential of currents as a function of the pH gradient. Symbols are individual data and the black horizontal lines are the mean. The dotted line is the expected reversal potential as predicted by the Nernst equation. The inset shows a tail current family from which instantaneous IV curves where extracted to measure the reversal potential. Recordings shown in A and B were obtained in the whole-cell configuration. C) Normalized conductance-voltage curve at ΔpH = 1. The red curve is the fit to equation 1 with parameters $V_{0.5}$ = 7.85 mV, q = 2.09 e_o. Circles are the mean and error bars are the s.e.m. (n = 7). D) Kinetic parameters of activation. Activation time constant and delay estimated from fits of current traces to equation 2. Circles are the mean and the s.e.m. is indicated by the shaded areas (n = 6). The voltage-dependence of the delay and tau of activation were estimated from a fit to

equation 3, which appears as the red curve. Parameters are: $\delta(0)$ = 98.2 ms, q_δ = 0.47 e_o. The voltage-dependence parameters for tau are: $\tau(0)$ = 212 ms, q_τ = 0.37 e_o.

Comparison to human H_v1 channel properties.

Human H_v1 is probably the best characterized of the voltage-gated proton channels (Musset et al., 2008), so we compared some of the properties of AmH_v1 with hH_v1. AmH_v1 channels activate faster than their human counterpart. Figure 3 compares the activation kinetics of these two channels under the same conditions. Steady-state is apparently reached sooner after a voltage pulse in AmH_v1 (Figure 3A) when compared to hH_v1 (Figure 3B). The slower kinetics of the human orthologue is also evidenced in the more sluggish deactivation tail currents (Figure 3B). The range of voltages over which activation happens is also different between the two channels, with the coral H_v1 channel activating 40 mV more negative than the human clone (Figure 3C. Notice that the proton gradient is the same in these recordings). Even though AmH_v1 activates at more negative voltages, the activation range is still more positive than the proton reversal potential, thus coral proton currents activated by depolarization, in the steady state and at least as expressed in HEK293 cells, are always outward.

The faster kinetics of AmH_v1 is clearly evidenced when the time constant of activation, τ, estimated using fits of the activation time course to equation 2, is compared for coral and human H_v1 channels. AmH_v1 is almost 10-fold faster at 0 mV and over a range of positive voltages (Figure 3D).

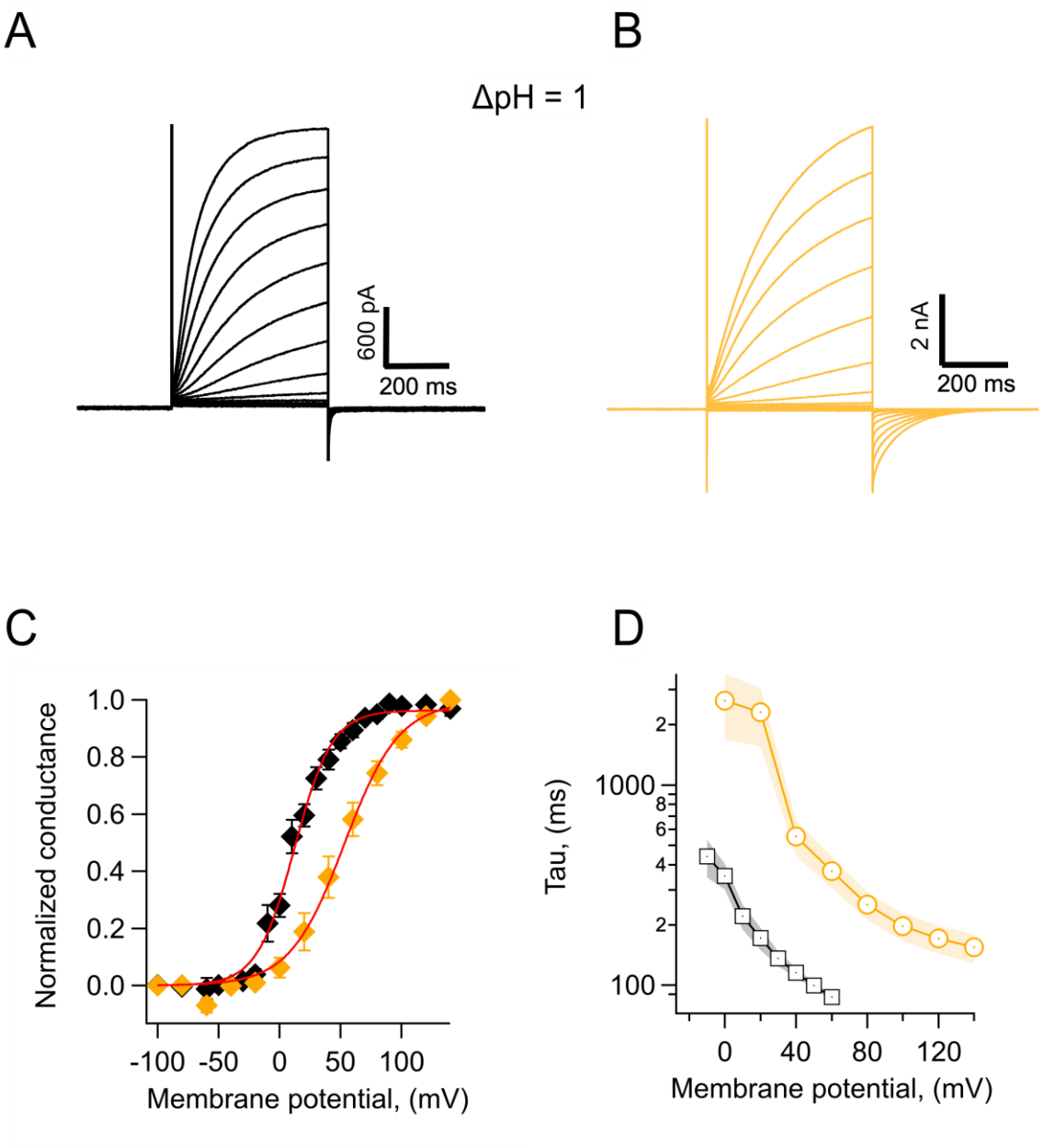

Figure 3

294

295 **Figure 3. Coral H_v1 channels are faster and activate more readily than their human**
296 **counterpart.** A) AmH_v1 currents in response to voltage-clamp pulses from -100 to 120 mV.
297 B) Currents through hH_v1 channels in response to voltage-clamp pulses from -100 to 120
298 mV. Recordings shown in A and B were obtained in whole-cell the configuration. C)

Comparison of the conductance-voltage relationship for both channels. Black diamonds are the mean G/G_{max} for AmH_v1 and yellow diamonds for hH_v1. The error bars are the s.e.m. (n= 3, for both channels). The continuous red curves are fits to equation 1. The fitted parameters are: AmH_v1, q = 1.62 e_o, $V_{0.5}$ =12.2 mV; hH_v1, q = 1.11 e_o, $V_{0.5}$ = 53.1 mV. D) The activation time constant estimated from fits of currents to equation 2. Circles are the mean for hH_v1 and squares for AmH_v1. The shaded areas are the s.e.m. (n= 3, for both channels).

Effects of the pH gradient on gating

Both native and cloned voltage-gated proton channels are characteristically modulated by the pH gradient (Cherny et al., 1995; Sasaki et al., 2006; Ramsey et al., 2006). We carried out experiments to investigate the modulation of the coral H_v1 channels by different pH gradients. We first recorded whole-cell currents at various ΔpH and estimated the voltage-dependence of the conductance. These G-V curves were fitted to equation 2 to obtain the voltage of half activation, $V_{0.5}$ and apparent gating charge, q, that determines the steepness of the fit. As is the case with other H_v1 channels, the $V_{0.5}$ shifts to negative voltages when ΔpH is greater that 0 and to positive voltages when ΔpH<0 (Figure 4A). When we plot the $V_{0.5}$ as a function of ΔpH the relationship seems to be mostly linear over the range of ΔpH -1 to 2. This relationship is somewhat steeper than the generally observed -40 mV/ΔpH (Figure 4B). We tried to obtain recordings over an extended range of ΔpH values. To this end, we performed inside-out recordings in which the composition of solutions can be better controlled, tend to be more stable and the size of currents is smaller. However, recordings were unstable at extreme pH values and we only managed to reliably extend the data to ΔpH of -2. Figure 4C shows the summary of the inside-out recordings. We have plotted both the $V_{0.5}$ and the threshold voltage, V_{Thr}. To obtain this last parameter, we fitted the exponential rise of the G-V curve to a function of the form:

$$G(V) = G' \cdot exp^{qV/K_BT}$$

V_{Thr} was calculated as the voltage at which the fit reaches 10 % of the maximum conductance. The parameter V_{Thr} should be less sensitive than $V_{0.5}$ to the possible change in the proton gradient that can occur with large currents. It is clear from these data that at extreme values

the dependence of $V_{0.5}$ or V_{Thr} on ΔpH deviates from a simple linear relationship and instead it appears to saturate with increasing ΔpH.

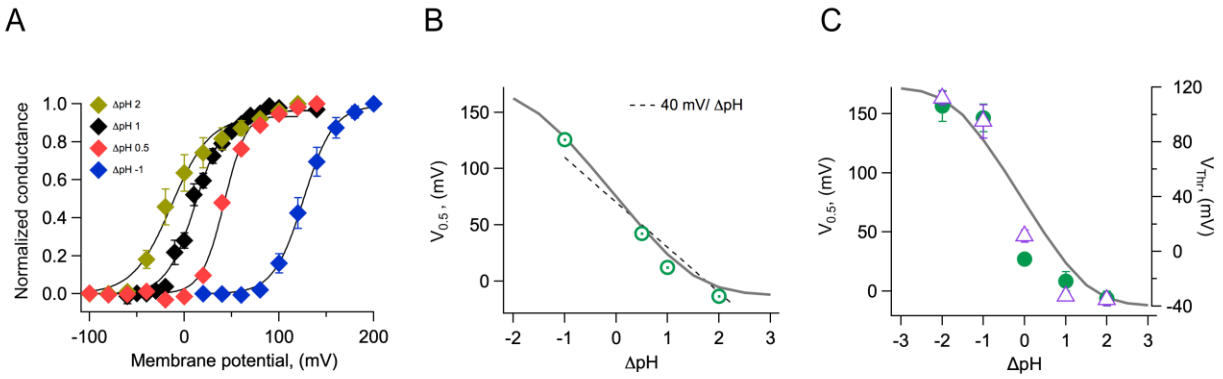

Figure 4. Modulation of channel activation by the pH gradient. A) Conductance vs. voltage relationships obtained at the indicated ΔpH values, obtained from whole-cell recordings of AmH_v1 proton currents. Continuous lines are fits to equation 1. B) The parameter $V_{0.5}$ was obtained from the fits in A and is displayed as a function of ΔpH. The dotted line is the 40 mV/ΔpH linear relationship. The continuous grey curve is the prediction of the allosteric model. C) Parameters $V_{0.5}$ (green circles) and V_{Thr} (purple triangles) obtained from a different set of inside-out current recordings. Data are mean ± s.e.m. The continuous grey curve is the same prediction of the allosteric model shown in B. The model parameters used to generate the theoretical curve are: $E=5x10^5$, $D=10^5$, $C=0.0002$, $Kv(0)=0.00005$, $q_g=1.0\ e_o$, $pK_o=3.4$, $pK_i=7$

Allosteric model of voltage and pH-dependent gating

Currently, there are is only one quantitative model that has been used to explain ΔpH gating of H_v1 channels (Cherny et al., 1995). However, this model is euristic and does not provide mechanistic insight into the process of proton modulation of the voltage dependence of proton permeable channels. In order to explain the modulation of the range of activation by the proton gradient, parameterized by the $V_{0.5}$, we developed a structurally-inspired allosteric model of voltage and proton activation. As many voltage-sensing domains, H_v1 has

two water-occupied cavities exposed to the extracellular and intracellular media (Ramsey et al., 2010; Islas and Sigworth, 2001; Ahern and Horn, 2005). Recent evidence suggests that these cavities function as proton-binding sites through networks of electrostatic interactions (De La Rosa et al., 2018). In our model, we propose that these two proton-binding sites, one intracellular and one extracellular, allosterically modulate the movement of the voltage-sensing S4 segment and thus channel activation in opposite ways. The extracellular site is postulated as inhibitory, while the intracellular site is excitatory, facilitating voltage sensor movement. As a first approximation, we employ a simplified allosteric formalism based on a Monod-Wyman-Changeux (MWC) style model (Horrigan and Aldrich, 2002; Changeux, 2012). As a simplifying assumption, in this model we assume that the voltage sensor moves in a single voltage-dependent activation step. We assume the external and an internal proton-binding sites have simple protonation given by a single pK_a value. These sites operate as two allosteric modules and are coupled to the voltage sensor according to coupling factors C and D, respectively. These binding sites in turn interact with each other through the coupling factor E. The modular representations of the model are illustrated in Figure 5A, while the full model depicting all open and closed states with all permissible transitions and the corresponding equilibrium constants for each transition is shown in Figure 5B. Full details of equations derived from these schemes are given in supplementary data.

This allosteric model represents a first attempt at producing a quantitative mechanistic understanding of the interaction of the voltage sensor and protons in H_v1 channels.

From the data shown in Figure 4C, it can be seen that the model is capable of reproducing the very steep dependence of $V_{0.5}$ on ΔpH and importantly, the saturation of this relationship at extreme values. Some H_v1 channels from other organisms show a linear dependence of gating over a large range of ΔpH values, while others show a reduced dependence and even saturation over some range of on ΔpH (Thomas et al., 2018). Our model can explain these different behaviors as different channels having distinct values of pk_as for the internal or external sites, differences in coupling factors or differences in the voltage-dependent parameters (Supplementary information).

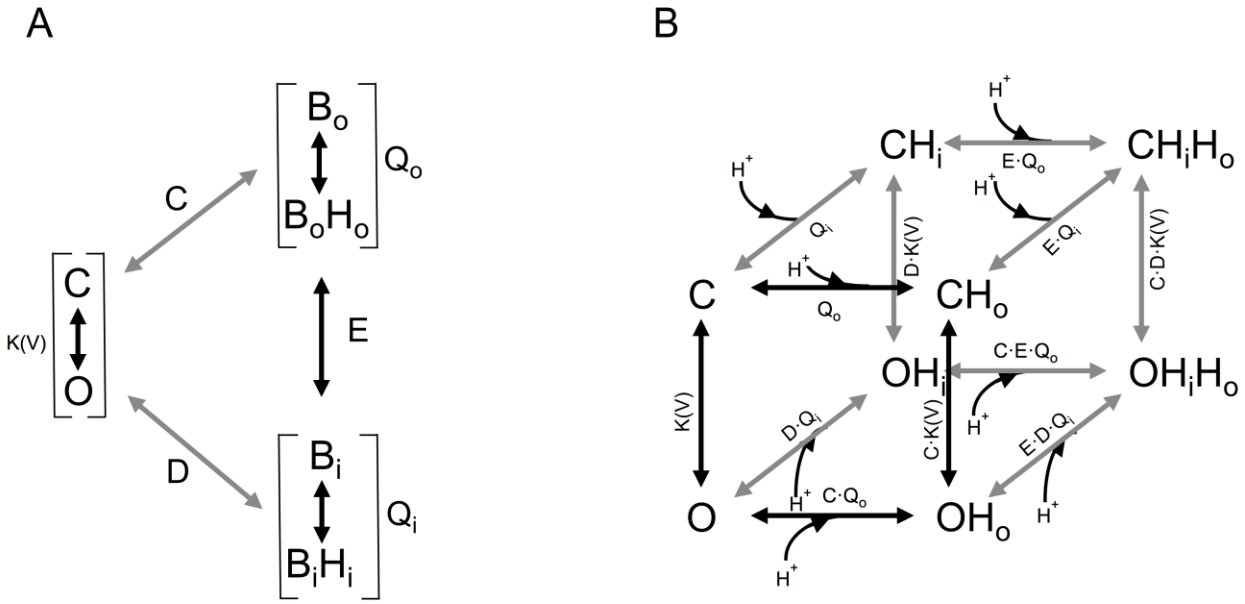

Figure 5. Gating scheme I. A) Modular representation of a simple MWC model; the channel opening transition is voltage-dependent, with equilibrium constant *K(V)*. B_o and B_i are the unbound states of the extracellular and intracellular proton-binding sites, respectively and B_oH_o and B_iH_i are the proton bound states of these binding sites. Q_o and Q_i are equilibrium constants that depend on the pK_a of each of these binding states. C, D and E are the coupling constants between each of the indicated modules.

B) All the individual states implied in A are depicted, along with proton-binding states and the appropriate equilibrium constants. C, closed states, O, open states. OH_x, OH_xH_x and CH_x, CH_xH_x are single or doubly proton-occupied states, where x can be o for outside or i for inside-facing binding sites.

Block by Zn^{2+}

The best characterized blocker of proton channels is the divalent ion zinc (Cherny et al., 2020; De La Rosa et al., 2018; Qiu et al., 2016). We performed experiments to determine if Am H_v1 channels are also inhibited by zinc. We found that indeed, extracellular application

of zinc in outside-out patches produced inhibition of the channels, reflected in reduced current amplitude (Figure 6A). Figure 6B shows average current-voltage relationships in the absence and presence of 10 μM external zinc. It can be seen that the fraction of current blocked is not the same at every voltage, indicating that this inhibition might be voltage-dependent. The fraction of blocked channels was calculated and is plotted at each voltage along with the I-V curves (Figure 6B). It can be clearly seen that inhibition by Zn^{2+} is voltage-dependent. A simple mechanism for voltage-dependent blockage was proposed by (Woodhull, 1973). This model postulates that a charged blocker molecule interacts with a binding site in the target molecule that is located within the electric field. Fitting the data according to this model, and given that zinc is a divalent ion, its apparent binding site is located at a fraction $\delta = 0.2$ of the membrane electric field from the extracellular side (Figure 6B).

Zinc blockage proceeds very fast. At 1 mM the channels are blocked almost instantaneously, and the inhibition washes off very fast as well (Figure 6C). Finally, we report the dose response curve (Figure 6D). The inhibition dose response curve can be fit by a Hill equation (Equation 4) with a slope factor of near 0.5 and an apparent dissociation constant, K_D of 27 μM.

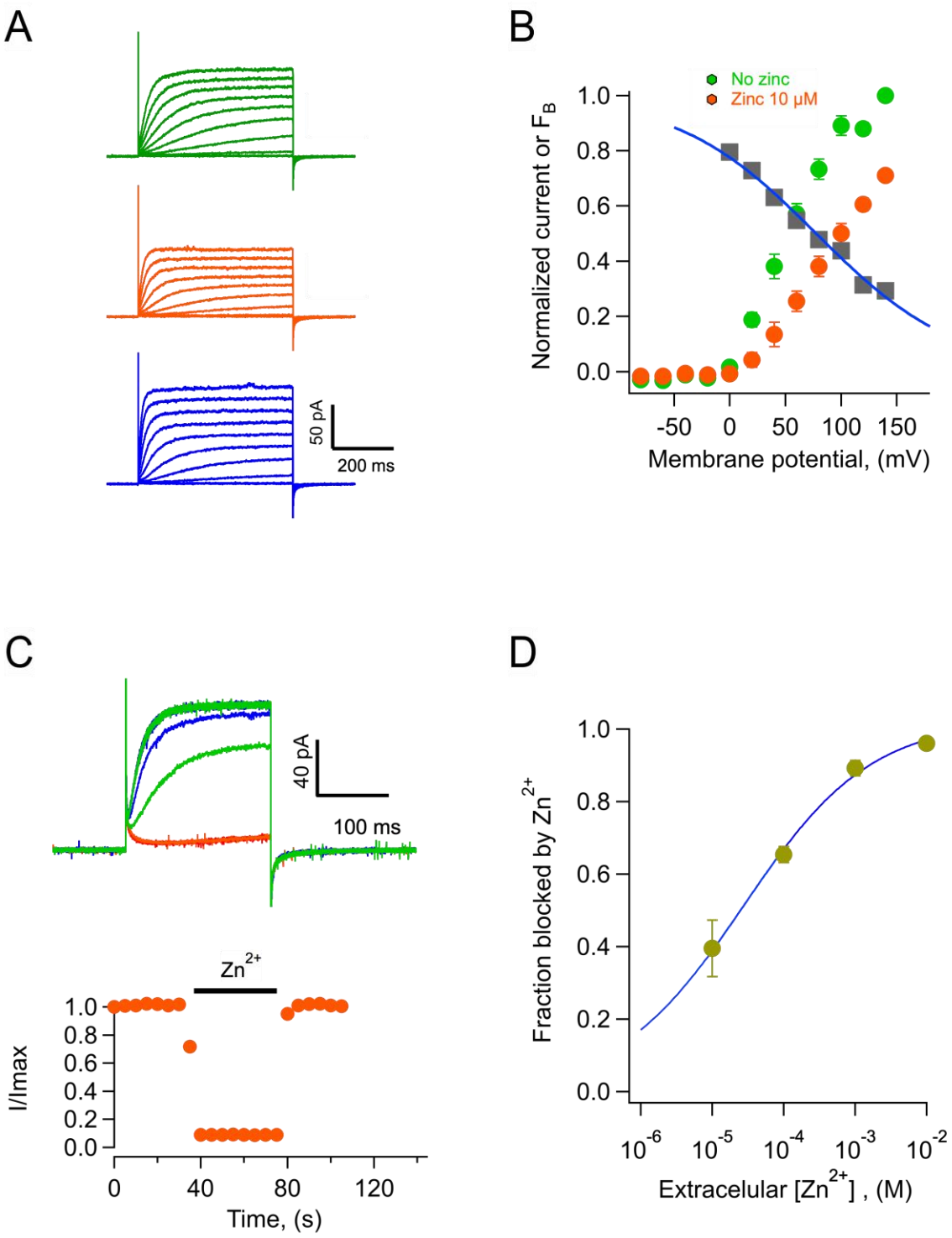

Figure 6. Block of AmH$_v$1 channels by extracellular zinc. A) AmH$_v$1-mediated currents from an outside-out patch in the absence (top), presence of 10 µM zinc (middle) and after washing of zinc (bottom). The scale bars apply to the three current families. B) Normalized current voltage relationships before and in the presence of 10 µM zinc from 4 patches as in

A. The grey squares are the ratio $I_{zinc}(V)/I(V)$, which gives the voltage-dependence of the blocking reaction. The blue curve is the fit to the Woodhull equation:

$F_B = \frac{1}{1+e^{-\delta z(V-V_{0.5})/K_BT}}$, where F_B is the fraction of current blocked, δ is the fraction of the electric field where the blocker binds, z is the valence of the blocker, $V_{0.5}$ is the potential where half of the current is blocked, K_B is Boltzmann's constant and T the temperature in Kelvin. The fitting parameters are: δ=0.19, $V_{0.5}$=77.6 mV. C) The effect of zinc is fast. Application of 1 mM zinc to an outside-out patch produces almost instantaneous block of ~90 % of the current. The effect also washes off quickly upon removal of zinc. Trace colors are as in A. Voltage pulse was 100 mV applied every 5 sec. D) Dose-response curve of zinc block of AmH_v1 obtained at 100 mV. The continuous curve is a fit of the data to equation 4 with apparent K_D = 27.4 μM and n = 0.48.

Discussion and conclusions

A few ion transport mechanisms in reef-building corals have been described, but up to now, no ion channels have been characterized from any scleractinian species. Here we show that voltage-gated proton-permeable channels formed by the H_v1 protein are present in corals. In particular, we have cloned these channels from two species of the genus *Acropora, A. millepora and A. palmata.* It is interesting that the protein sequence of these proteins shows a very high degree of conservation, suggesting that, even when the two species are found in different oceans, they haven't had time to diverge substantially or alternatively, selective pressures on these channels are very similar in both species. The presence of H_v1 sequences in many other species of corals from disparate clades, suggest that H_v1 plays an important role in coral physiology.

Our experiments show that these coral proteins give rise to proton currents when expressed in HEK293 cells and we present a characterization of some of their biophysical properties. These channels retain the functional characteristics that have been shown to define the class in other species, such as very high selectivity for protons, activation by voltage and modulation of this activation by the proton gradient. The new channels reported here activate faster that the human H_v1 channel. It has been known that different orthologs of H_v1

activate with varying kinetics. For example, sea urchin, dinoflagellate and recently, fungal H_v1 channels activate rapidly, while most mammalian counterparts have slow activation rates (Musset et al., 2008; Smith et al., 2011; Zhao and Tombola, 2021). A comparative study suggests that two amino acids in the S3 transmembrane segment are important determinants of kinetic differences between sea urchin and mouse H_v1 (Sakata et al., 2016). The authors suggest that the time course of activation is slow in channels containing a histidine and a phenylalanine at positions 164 and 166, respectively (mouse sequence numbering). The AmH_v1 has a histidine at equivalent position 132 and a methionine at 134. It is possible that this last amino acid in AmH_v1 confers most of the fast kinetics phenotype. A separate work showed that a lack of the amino-terminal segment in human sperm H_v1 also produced fast-activating channels (Berger et al., 2017). Interestingly, the *Acropora* channels have a shorter amino-terminal sequence, which could also contribute to their fast kinetics.

One of the most interesting characteristics found in these new proton channels is their modulation by the proton gradient. As opposed to other H_v1 channels, we can observe a trend towards saturation of the $V_{0.5}$ for activation as a function of ΔpH at extreme values of this variable. A tendency towards saturation of the $V_{0.5}$-ΔpH relationship has been observed in mutants of the hH_v1 channel (Cherny et al., 2015) or at negative values of ΔpH for a snail H_v1 (Thomas et al., 2018), but it seems it can be fully appreciated in AmH_v1. Since our model explains the observation of saturation of voltage gating at extreme values of ΔpH as a consequence of the existence of two saturable sites for proton binding, we attribute this behavior, to the large separation of pK_a values for the extracellular and intracellular proton binding sites.

The strength of allosteric coupling of these sites and the voltage sensor will determine if saturation is observed over a short or extended range of ΔpH values and the range of values of $V_{0.5}$ that a particular channel can visit. Our model should provide a framework to better understand gating mechanisms in future work.

It is clear that more complicated models, with a larger number of voltage dependent and independent steps (Villalba-Galea, 2014) and coupling to protonation sites should be the next step to improve data fitting and explore voltage-and proton-dependent kinetics. In

particular, these types of models can help explain mutagenesis experiments exploring the nature of the protonation sites.

What is the function of voltage-gated proton channels in corals? The deposition of a $CaCO_3$ exoskeleton is one of the main defining characteristics of scleractinians, however, the ionic transport mechanisms involved in this process are mostly unknown. In order for aragonite precipitation to occur favorably, the pH of the calicoblastic fluid, right next to the skeleton is maintained at high levels, between 8.5 and 9 and above the pH of sea water (Le Goff et al., 2017). It has been posited that corals control this pH via vectorial transport of protons to the gastrodermal cavity (Jokiel, 2013). Since proton transport away from the site of calcification would incur a drastically lower intracellular pH in the cells of the aboral region, we propose that, given their ability to rapidly regulate intracellular pH (De la Rosa et al., 2016), H_v1 proton channels contribute by transporting protons from the cells. Thus, these proton channels would be a major component of the mechanisms of intracellular pH regulation. Given that the activation range of H_v1 is controlled by the pH gradient, a large intracellular acidification would facilitate opening of these channels at the resting potential of cells, which is presumably negative.

The finding that coral H_v1 channels retain their sensitivity to Zn^{2+}, opens the possibility of using this ion as a pharmacological tool to study the role of proton channels in pH homeostasis. It is interesting that a recent report has shown detrimental effects of zinc supplementation in coral growth (Tijssen et al., 2017), a result that could be explained by zinc inhibition of H_v1.

The physiological role of H_v1 channels in corals might be essential in the response of these organisms to ocean acidification. We theorize that as the pH of sea water acidifies, gating of H_v1 should require stronger depolarization, thus hindering its capacity to transport protons from the cell. This will contribute to a diminished calcification rate and less aragonite saturation of the $CaCO_3$ skeleton. It would be interesting and important to study the effects of acidification on H_v1 physiology and pH regulation in corals in vivo. Essentially nothing is known about the electrophysiological properties of coral cells. This report represents the first time that an ion channel has been cloned and characterized in any coral and should open

a new avenue of research, such as uncovering the cellular and possible subcellular localization of these channels and carefully measuring their physiological role in vivo.

Acknowledgments. We would like to thank Alejandra Llorente for excellent technical assistance. This work was funded in part by grant No. IN215621 from DGAPA-PAPIIT-UNAM to L.D.I., grant No. 247765 to A.T.B. and grant No. IN200720 to T.R.

Author contributions. G.R-Y, performed cloning, performed heterologous expression, performed experiments, read the paper. C.C., M.A.C.-R., E.S-D., performed cloning, expression and electrophysiology experiments. L.D.I. obtained funding, conceived research, procured animals, analyzed data, wrote the paper. A.B. and E.M. procured collection permits and specimens, performed RNA extraction, revised and edited the paper. I.S.R. contributed ideas, revised and edited the paper. T.R. wrote the paper, contributed ideas.

References

Ahern, C.A., and R. Horn. 2005. Focused electric field across the voltage sensor of potassium channels. *Neuron*. 48:25–29.

Allemand, D., É. Tambutté, D. Zoccola, and S. Tambutté. 2011. Coral calcification, cells to reefs. *Coral Reefs Ecosyst. Transit.* 119–150.

Berger, T.K., D.M. Fußhöller, N. Goodwin, W. Bönigk, A. Müller, N. Dokani Khesroshahi, C. Brenker, D. Wachten, E. Krause, and U.B. Kaupp. 2017. Post-translational cleavage of Hv1 in human sperm tunes pH-and voltage-dependent gating. *J. Physiol.* 595:1533–1546.

Carmona, E.M., H.P. Larsson, A. Neely, O. Alvarez, R. Latorre, and C. Gonzalez. 2018. Gating charge displacement in a monomeric voltage-gated proton (H_v1) channel. *Proc. Natl. Acad. Sci.* 115:9240–9245. doi:10.1073/pnas.1809705115.

Castillo, K., A. Pupo, D. Baez-Nieto, G.F. Contreras, F.J. Morera, A. Neely, R. Latorre, and C. Gonzalez. 2015. Voltage-gated proton (Hv1) channels, a singular voltage sensing domain. *FEBS Lett.* 589:3471–3478.

Changeux, J.-P. 2012. Allostery and the Monod-Wyman-Changeux model after 50 years. *Annu. Rev. Biophys.* 41:103–133.

Cherny, V.V., V.S. Markin, and T.E. DeCoursey. 1995. The voltage-activated hydrogen ion conductance in rat alveolar epithelial cells is determined by the pH gradient. *J. Gen. Physiol.* 105:861–896.

Cherny, V.V., D. Morgan, B. Musset, G. Chaves, S.M. Smith, and T.E. DeCoursey. 2015. Tryptophan 207 is crucial to the unique properties of the human voltage-gated proton channel, hHV1. *J. Gen. Physiol.* 146:343–356.

Cherny, V.V., R. Murphy, V. Sokolov, R.A. Levis, and T.E. DeCoursey. 2003. Properties of single voltage-gated proton channels in human eosinophils estimated by noise analysis and by direct measurement. *J. Gen. Physiol.* 121:615–628.

Cherny, V.V., B. Musset, D. Morgan, S. Thomas, S.M. Smith, and T.E. DeCoursey. 2020. Engineered high-affinity zinc binding site reveals gating configurations of a human proton channel. *J. Gen. Physiol.* 152.

Chomczynski, P., and N. Sacchi. 1987. Single-step method of RNA isolation by acid guanidinium thiocyanate-phenol-chloroform extraction. *Anal. Biochem.* 162:156–159.

De La Rosa, V., A.L. Bennett, and I.S. Ramsey. 2018. Coupling between an electrostatic network and the Zn2+ binding site modulates Hv1 activation. *J. Gen. Physiol.* 150:863–881.

De La Rosa, V., and I.S. Ramsey. 2018. Gating currents in the Hv1 proton channel. *Biophys. J.* 114:2844–2854.

De la Rosa, V., E. Suárez-Delgado, G.E. Rangel-Yescas, and L.D. Islas. 2016. Currents through Hv1 channels deplete protons in their vicinity. *J. Gen. Physiol.* 147:127–136.

DeCoursey, T.E. 2013. Voltage-gated proton channels: molecular biology, physiology, and pathophysiology of the HV family. *Physiol. Rev.* 93:599–652.

Horrigan, F.T., and R.W. Aldrich. 2002. Coupling between voltage sensor activation, Ca2+ binding and channel opening in large conductance (BK) potassium channels. *J. Gen. Physiol.* 120:267–305.

Islas, L.D., and F.J. Sigworth. 2001. Electrostatics and the gating pore of Shaker potassium channels. *J. Gen. Physiol.* 117:69–90.

Jokiel, P.L. 2013. Coral reef calcification: carbonate, bicarbonate and proton flux under conditions of increasing ocean acidification. *Proc. R. Soc. B Biol. Sci.* 280:20130031.

Le Goff, C., E. Tambutté, A.A. Venn, N. Techer, D. Allemand, and S. Tambutté. 2017. In vivo pH measurement at the site of calcification in an octocoral. *Sci. Rep.* 7:1–14.

Lishko, P.V., and Y. Kirichok. 2010. The role of Hv1 and CatSper channels in sperm activation. *J. Physiol.* 588:4667–4672.

Long, S.B., E.B. Campbell, and R. MacKinnon. 2005. Crystal structure of a mammalian voltage-dependent Shaker family K+ channel. *Science*. 309:897–903.

McDonnell, A.V., T. Jiang, A.E. Keating, and B. Berger. 2006. Paircoil2: improved prediction of coiled coils from sequence. *Bioinformatics*. 22:356–358.

Moya, A., L. Huisman, E.E. Ball, D.C. Hayward, L.C. Grasso, C.M. Chua, H.N. Woo, J.-P. Gattuso, S. Foret, and D.J. Miller. 2012. Whole transcriptome analysis of the coral Acropora millepora reveals complex responses to CO2-driven acidification during the initiation of calcification. *Mol. Ecol.* 21:2440–2454.

Musset, B., V.V. Cherny, D. Morgan, Y. Okamura, I.S. Ramsey, D.E. Clapham, and T.E. DeCoursey. 2008. Detailed comparison of expressed and native voltage-gated proton channel currents. *J. Physiol.* 586:2477–2486.

Qiu, F., A. Chamberlin, B.M. Watkins, A. Ionescu, M.E. Perez, R. Barro-Soria, C. González, S.Y. Noskov, and H.P. Larsson. 2016. Molecular mechanism of Zn2+ inhibition of a voltage-gated proton channel. *Proc. Natl. Acad. Sci.* 113:E5962–E5971.

Ramsey, I.S., Y. Mokrab, I. Carvacho, Z.A. Sands, M.S. Sansom, and D.E. Clapham. 2010. An aqueous H+ permeation pathway in the voltage-gated proton channel Hv1. *Nat. Struct. Mol. Biol.* 17:869.

Ramsey, I.S., M.M. Moran, J.A. Chong, and D.E. Clapham. 2006. A voltage-gated proton-selective channel lacking the pore domain. *Nature*. 440:1213–1216.

Randolph, A.L., Y. Mokrab, A.L. Bennett, M.S. Sansom, and I.S. Ramsey. 2016. Proton currents constrain structural models of voltage sensor activation. *Elife*. 5:e18017.

Sakata, S., N. Miyawaki, T.J. McCormack, H. Arima, A. Kawanabe, N. Özkucur, T. Kurokawa, Y. Jinno, Y. Fujiwara, and Y. Okamura. 2016. Comparison between mouse and sea urchin orthologs of voltage-gated proton channel suggests role of S3 segment in activation gating. *Biochim. Biophys. Acta BBA-Biomembr.* 1858:2972–2983.

Sasaki, M., M. Takagi, and Y. Okamura. 2006. A voltage sensor-domain protein is a voltage-gated proton channel. *Science*. 312:589–592.

Schoppa, N.E., and F.J. Sigworth. 1998. Activation of Shaker potassium channels: I. Characterization of voltage-dependent transitions. *J. Gen. Physiol.* 111:271–294.

Smith, S.M.E., D. Morgan, B. Musset, V.V. Cherny, A.R. Place, J.W. Hastings, and T.E. DeCoursey. 2011. Voltage-gated proton channel in a dinoflagellate. *Proc. Natl. Acad. Sci.* 108:18162–18167. doi:10.1073/pnas.1115405108.

609 Takeshita, K., S. Sakata, E. Yamashita, Y. Fujiwara, A. Kawanabe, T. Kurokawa, Y. Okochi, M.
610 Matsuda, H. Narita, and Y. Okamura. 2014a. X-ray crystal structure of voltage-gated
611 proton channel. *Nat. Struct. Mol. Biol.* 21:352–357.

612 Takeshita, K., S. Sakata, E. Yamashita, Y. Fujiwara, A. Kawanabe, T. Kurokawa, Y. Okochi, M.
613 Matsuda, H. Narita, Y. Okamura, and A. Nakagawa. 2014b. X-ray crystal structure of
614 voltage-gated proton channel. *Nat. Struct. Mol. Biol.* 21:352–357.
615 doi:10.1038/nsmb.2783.

616 Taylor, A.R., A. Chrachri, G. Wheeler, H. Goddard, and C. Brownlee. 2011. A voltage-gated H+
617 channel underlying pH homeostasis in calcifying coccolithophores. *PLoS Biol*.
618 9:e1001085.

619 Thomas, S., V.V. Cherny, D. Morgan, L.R. Artinian, V. Rehder, S.M. Smith, and T.E. DeCoursey.
620 2018. Exotic properties of a voltage-gated proton channel from the snail Helisoma
621 trivolvis. *J. Gen. Physiol.* 150:835–850.

622 Tijssen, J., T. Wijgerde, M.C. Leal, and R. Osinga. 2017. Effects of zinc supplementation on
623 growth and colouration of the scleractinian coral Stylophora pistillata. PeerJ
624 Preprints.

625 Tresguerres, M., K.L. Barott, M.E. Barron, D.D. Deheyn, D.I. Kline, and L.B. Linsmayer. 2017.
626 Cell biology of reef-building corals: ion transport, acid/base regulation, and energy
627 metabolism. *Acid-Base Balance Nitrogen Excretion Invertebr.* 193–218.

628 Villalba-Galea, C.A. 2014. Hv1 proton channel opening is preceded by a voltage-
629 independent transition. *Biophys. J.* 107:1564–1572.

630 Waterhouse, A., M. Bertoni, S. Bienert, G. Studer, G. Tauriello, R. Gumienny, F.T. Heer, T.A.P.
631 de Beer, C. Rempfer, and L. Bordoli. 2018. SWISS-MODEL: homology modelling of
632 protein structures and complexes. *Nucleic Acids Res.* 46:W296–W303.

633 Woodhull, A.M. 1973. Ionic blockage of sodium channels in nerve. *J. Gen. Physiol.* 61:687–
634 708.

635 Zhao, C., and F. Tombola. 2021. Voltage-gated proton channels from fungi highlight role of
636 peripheral regions in channel activation. *Commun. Biol.* 4:1–13.

637

638

639

640

641

642

643 **Table 1.**

Oligo name	Sequence
AcHvNt5´	ATGATTGATGCAAGAACCAGACGATCGAGCATGGATGAT
AcHvNt3´	TGATCCTGCTCTCAAGTCAAGAACCAACTCAGCAATGAC
AcHvCt5´	ATGGGATTCACATTTTCAAGCACAAATGGAGGTGTTT
AcHvCt3´	TCAGCTTTGTTTTAATGTTGTCAATTCAGACTCCAACTG

644 Oligonucleotides used to clone amino and carboxy terminal partial sequences of AmH_v1 from
645 total reverse-transcribed mRNA from *A. millepora*.
646
647
648
649
650
651
652
653
654
655
656
657
658
659
660
661
662
663
664
665
666
667

Supplementary materials.

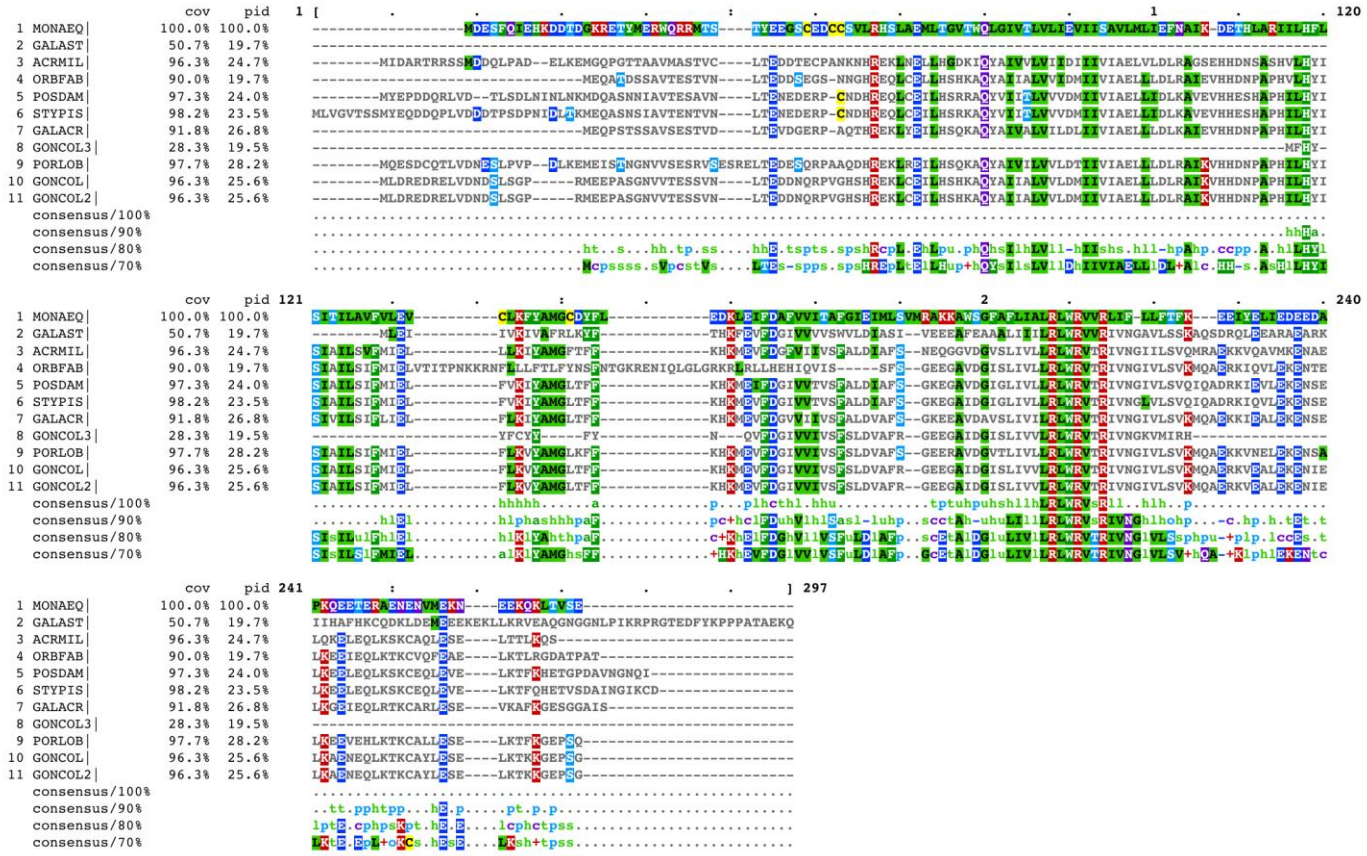

Supplementary Figure 1. Comparison of the AmH$_V$1 protein sequence with similar sequences found in other coral species. MONAEQ: *Montastrea*. GALAST:*Galastrea*. ACRMIL: *Acropora millepora*. ORBFAB: *Orbicela faveolata*. POSDAM: *Posillopora damicornis*. STYPIS: *Stylophora pistilata*. GALACR: *Galaxea*. GONCOL: *Goniopora*. PORLOB: *Porites lobata.*

A

```
Ap MIDARTRRSSMDDQLPADELKEMGQPGTTAAVMASTVCLTEDDTECPANKNHREKLNELL
Am MIDARTRRSSMDDQLPADELKEMGQPGTTAAVMASTVCLTEDDTECPANKNHREKLNELL
   ************************************************************

Ap HGDKIQYAIVVLVIIDIIIVIAELVLDSRAGSEHHDNSASHVLHYISIAILSVFMIELLL
Am HGDKIQYAIVVLVIIDIIIVIAELVLDLRAGSEHHDNSASHVLHYISIAILSVFMIELLL
   *************************** ********************************

Ap KIYAMGFTFFKHKMEVFDGFVIIVSFALDIAFSNEQGGVDGVSLIVLLRLWRVTRIVNGI
Am KIYAMGFTFFKHKMEVFDGFVIIVSFALDIAFSNEQGGVDGVSLIVLLRLWRVTRIVNGI
   ************************************************************

Ap ILSVQMRAERKVQAVTKENAELKEELEQLKSKCAQLESELTTLKQS
Am ILSVQMRAEKKVQAVMKENAELQKELEQLKSKCAQLESELTTLKQS
   ********* ***** ****** ***********************
```

B

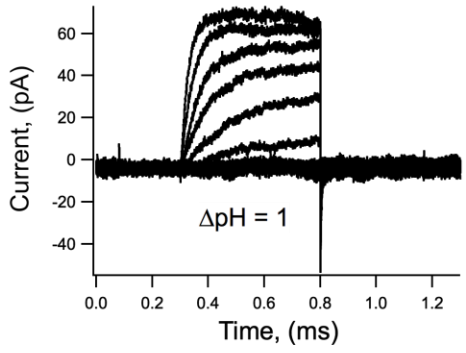

C

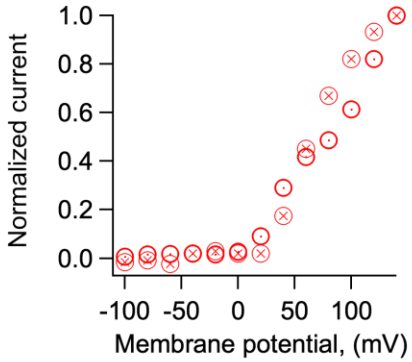

Supplementary Figure 2

Supplementary Figure 2. Some characteristics of the H_v1 from *Acropora palmata*. A) Comparison of the amino acid sequence of H_v1s from *Acropora millepora* (Am) and *Acropora palmata* (Ap). The asterisks bellow each residue indicate identity. B) Currents elicited from an inside-out patch obtained from a HEK293 cell expressing ApH_v1. Voltage pulses were from -100 to 140 mV in 20 mV steps. The ΔpH was 1. C) Normalized current-voltage relationships of two patches obtained as in B.

Supplementary data. Model equations and simulations.

The full complement of discrete states in our model is shown in Scheme I. This allosteric model predicts that the open probability, *P(V, pH)* is dependent on voltage and pH according to the following equations:

$$P(V,pH) = \frac{K_v \cdot \Omega}{K_v \cdot \Omega + \Gamma}$$

Where:

$$\Omega = 1 + Q_o C + Q_i D + Q_o Q_i i DEC$$

$$\Gamma = 1 + Q_o + Q_i + Q_o Q_i i E$$

$$K(V) = K(0) \cdot e^{\left(q_g V / K_B T\right)}$$

$$Q_o = \frac{1}{1 + 10^{(pH_o - pK_o)}}$$

$$Q_i = \frac{1}{1 + 10^{(pH_i - pK_i)}}$$

The voltage of half activation is given by:

$$V_{0.5} = \frac{K_B T}{q_g} \cdot ln\left(\frac{\Gamma}{K(0) \cdot \Omega}\right)$$

pK_o and pK_i are the pK_a values of the extracellular and intracellular proton binding sites, respectively.

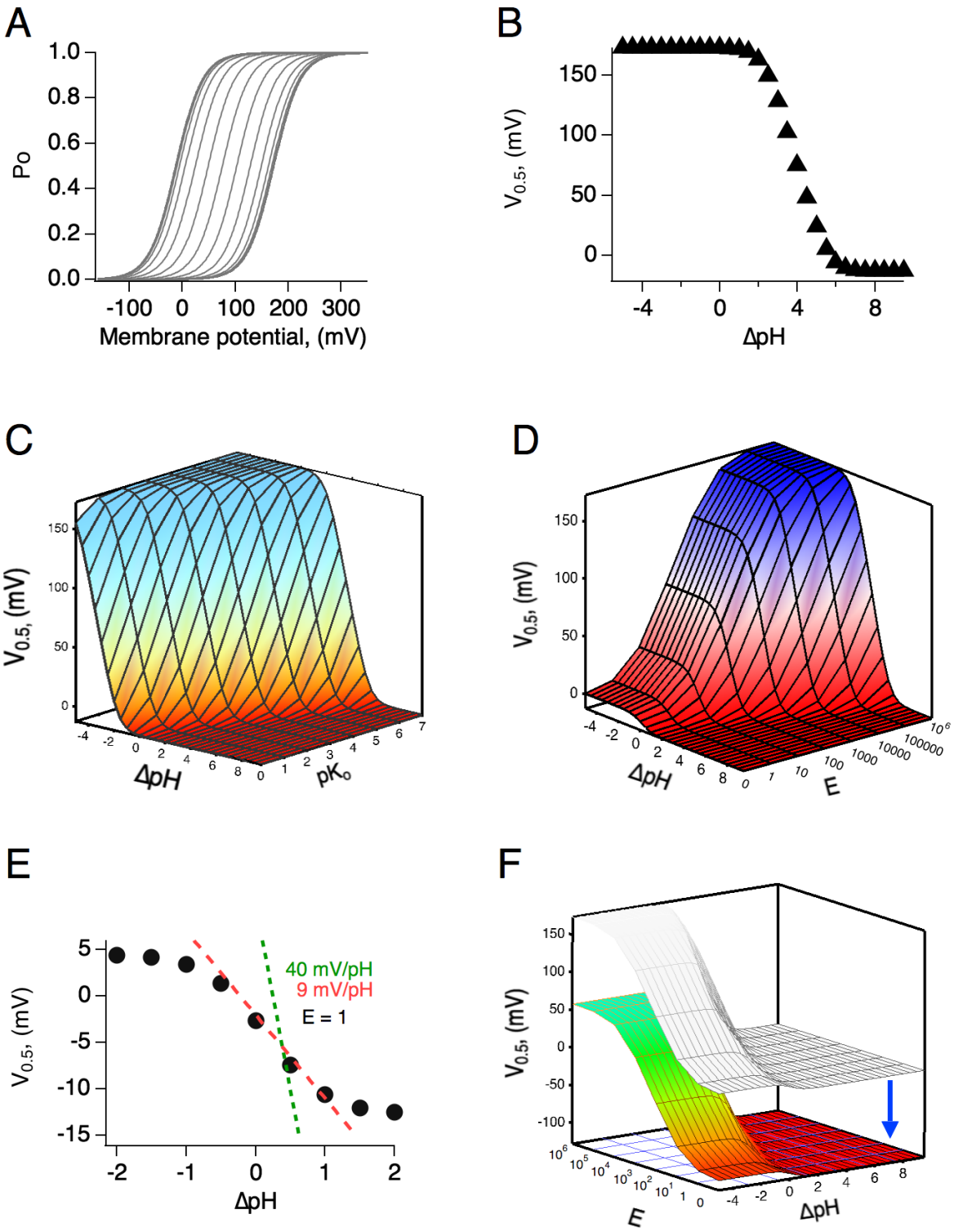

Supplementary figure 3. Simulations of the voltage- and pH-dependent behavior predicted by the allosteric model. A) Calculated GV curves and B) $V_{0.5}$ as a function of ΔpH. Model

parameters are: pK_o, pK_i = 7, K(0) = 0.00005, q = 1 e_o, E = 10^6, C = 0.0002, D = 10^5. C) $V_{0.5}$ as a function of ΔpH calculated for different values of the pK_o. D) $V_{0.5}$ as a function of ΔpH calculated for different values of the coupling factor E, which determines the allosteric communication between external and internal protonation sites. Note that lack of coupling between sites (E = 1), results in channels with very shallow modulation by pH, as illustrated in E. All other parameters are as in A and B. E) A slice of the surface in D, with E =1. The two lines show the expected dependence of $V_{0.5}$ on ΔpH for a fully modulated channel (E>100). Also shown is the dependence of 9 mV/ΔpH unit. F) The range of $V_{0.5\ is}$ dependent on the value of the voltage-dependent equilibrium constant at 0 mV. An increase to K(0)=0.005 shifts the whole surface by approximately -110 mV. All other parameters are as in D.